A Pseudo-Michaelis Quaternary Complex in the Reverse Reaction of a Ligase: Structure of *Escherichia coli* B Glutathione Synthetase Complexed with ADP, Glutathione, and Sulfate at 2.0 Å Resolution[†,‡]

Takane Hara,[§] Hiroaki Kato,[§] Yukiteru Katsube,[||] and Jun'ichi Oda*[,§]

Institute for Chemical Research, Kyoto University, Uji, Kyoto 611, Japan, and Institute for Protein Research, Osaka University, Suita, Osaka 565, Japan

Received March 4, 1996; Revised Manuscript Received June 7, 1996[⊗]

ABSTRACT: The crystal structure of glutathione synthetase from *Escherichia coli* B complexed with ADP, glutathione, and sulfate has been determined at 2.0 Å resolution. Concerning the chemical similarity of sulfate and phosphate, this quaternary complex structure represents a pseudo enzyme−substrate complex in the reverse reaction and consequently allows us to understand the active site architecture of the *E. coli* glutathione synthetase. Two Mg^{2+} ions are coordinated with oxygen atoms from the α- and β-phosphate groups of ADP and from the sulfate ion. The flexible loops, invisible in the unliganded or the binary and ternary complex structures, are fixed in the quaternary complex. The larger flexible loop (Ile226−Arg241) includes one turn of a 3_{10}-helix that comprises the binding site of the glycine moiety of GSH. The small loop (Gly164−Gly167) is involved in nucleotide binding and acts as a phosphate gripper. The side chains of Arg210 and Arg225 interact with the sulfate ion and the β-phosphate moiety of ADP. Arg 210 is likely to interact with the carboxylate of the C-terminal γ-glutamylcysteine in the substrate-binding form of the forward reaction. Other positively charged residues in the active site (Lys125 and Lys160) are involved in nucleotide binding, directing the phosphate groups to the right position for catalysis. Functional aspects of the active site architecture in the substrate-binding form are discussed.

Glutathione synthetase [γ-L-glutamyl-L-cysteine:glycine ligase (ADP-forming), EC 6.3.2.3] (GSHase)[1] is ubiquitous and present in a wide diversity among bacteria, plants, and mammals (Meister, 1988). GSHase catalyzes the ligation of γ-L-glutamyl-L-cysteine (γ-Glu-Cys) and Gly with the aid of ATP in the presence of Mg^{2+} ion. The reaction has been proposed to proceed via the phosphorylation of the C-terminal carboxylate of γ-Glu-Cys by the γ-phosphate group of ATP to form an acyl phosphate intermediate, followed by nucleophilic attack of glycine to produce glutathione (GSH), ADP, and inorganic phosphate (Scheme 1). A group of C−N bond ligases takes a similar route to activate a carboxylate group by phosphoryl transfer, yielding the aminoacyl phosphate intermediate. This family includes glutamine synthetase (EC 6.3.1.2), γ-Glu-Cys synthetase (EC 6.3.2.2), and D-Ala:D-Ala ligase (EC 6.3.2.4). The kinetic mechanism for glutamine synthetase and D-Ala:D-Ala ligase has been determined to be an ordered Ter-Ter reaction, where ATP is the first bound substrate and ADP is the last released product (Meek & Villafranca, 1980; Mullins et al., 1990). The initial velocity studies indicate that a central quaternary complex is present during the reaction since no product is released prior to the binding of all substrates. The *Escherichia coli* GSHase also shows a similar sequential mechanism (unpublished data); however, the order of the substrate binding and product release is still unclear.

Scheme 1

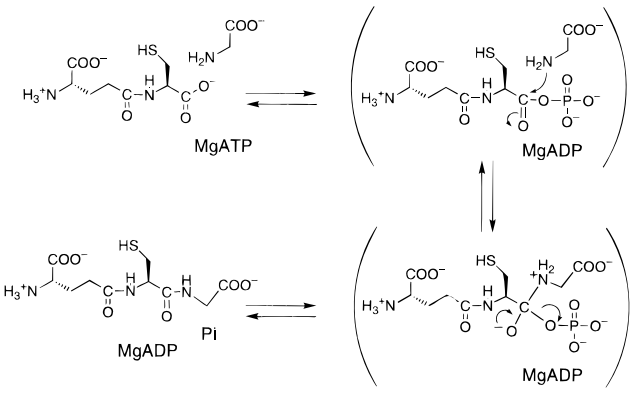

The *E. coli* GSHase is a tetramer, and each subunit is composed of 316 amino acid residues (Gushima et al., 1983, 1984). The three-dimensional structure of the unliganded GSHase has been determined at 2.0 Å resolution (Yamaguchi et al., 1993). In its structure, two peptide regions from Gly164 to Gly167 (the small loop) and from Ile226 to Arg241 (the large loop) are invisible in the electron density map because of the disordered or flexible nature of these two loops. The large loop seems to extend over the bound substrates in the active site to move from an "open" position in the unliganded enzyme into a "closed" position in the case of the enzyme with substrates bound at the active site

[†] This work was supported in part by Grants-in-Aid for Scientific Research from the Ministry of Education, Science and Culture of Japan. T.H. was a recipient of a research fellowship from the Japanese Society for the Promotion of Science for Young Scientists. Data collection at the Photon Factory was performed under Program 91-042.

[‡] The crystallographic coordinates have been deposited in the Brookhaven Protein Data Bank (code: 1GSA).

* To whom correspondence should be addressed.

[§] Kyoto University.

[||] Osaka University.

[⊗] Abstract published in *Advance ACS Abstracts,* August 15, 1996.

[1] Abbreviations: GSHase, glutathione synthetase; GSH, glutathione; γ-Glu-Cys, γ-L-glutamyl-L-cysteine; *E. coli*, *Escherichia coli*; SA, simulated annealing; RMS, root mean square.

S0006-2960(96)00524-7 CCC: $12.00

(Tanaka et al., 1992, 1993). The studies of a loopless mutant enzyme, in which the large loop was replaced with three glycine residues, indicated that the large loop functions to enhance the recognition of the substrate glycine as well as to stabilize the acylphosphate intermediate so that the intermediate reacts with glycine rapidly (Kato et al., 1994).

Approximate locations of the ATP- and γ-Glu-Cys-binding sites have been indicated by difference Fourier analysis of GSHase complexed with ATP and/or a γ-Glu-Cys analog, γ-L-glutamyl-α-L-aminobutyrate (Yamaguchi et al., 1993). The location of the ATP-binding site has been also deduced by the other crystallographic analysis of the enzyme covalently attached to adenosine(5′)tetraphosphopyridoxal (Hibi et al., 1993). The ATP molecule is surrounded by two sets of the structural motifs: an antiparallel β-sheet and a glycine-rich loop, the large or the small loop. The former motif is present commonly in the non-Rossmann fold type structures of nucleotide-dependent enzymes (Cusack et al., 1990; Knighton et al., 1991a,b; Ruff et al., 1991; Fan et al., 1994). One of the residues involved in the binding of the γ-Glu-Cys molecule was pointed out to be Arg86 by site-directed mutagenesis (Hara et al., 1995). However, the binary and ternary crystal structures of GSHase complexed with ATP and/or the γ-Glu-Cys analog provide clear electron density only for the adenosyl portion of ATP but ambiguous density for the phosphate moieties, the γ-Glu-Cys analog, and the two flexible loop regions. This observation is attributed to the absence of interactions between the bound substrates, Mg^{2+} ion, the phosphate moieties of ATP, and the loops. In light of the kinetic mechanism, we believe that the formation of the quaternary E−S complex is necessary to induce a fully ordered structure at the active site.

This paper describes the refined crystal structure of the *E. coli* GSHase complexed with ADP, GSH, two Mg^{2+} ions, and one sulfate ion bound at the active site. The complex represents a pseudo-Michaelis complex in the reverse reaction of GSHase since sulfate mimics phosphate, one of the substrates in the reverse reaction. Refinement of this structure allowed us to model the missing loop structures in the electron density map. The structure provides an insight to understand the architecture of the active site of GSHase and to implicate residues in the substrate recognition mechanism.

MATERIALS AND METHODS

Materials. Plasmid pKGS00 is a pKK233-3 derivative containing a 1.2 kilobase pair fragment of the GSHase gene (*gsh-II*) from *E. coli* B (Kato et al., 1988). *E. coli* JM109 was provided by Takara Shuzo Co., Ltd. (Kyoto, Japan). ADP was obtained from Oriental Yeast Co., Ltd. (Tokyo, Japan). GSH was purchased from Kokusan Chemicals Co., Ltd. (Tokyo, Japan). Chemicals used in this experiment were of the purest grade commercially available.

Purification and Crystallization. *E. coli* JM109 containing the plasmid pKGS00 was used as an overexpressing clone. Purification of GSHase was performed according to the procedure previously described (Kato et al., 1989). The purified preparation was dialyzed against 50 mM Tris-HCl buffer (pH 7.5) containing 5 mM $MgCl_2$ and stored at 4 °C. Purity of the preparation was checked by SDS−polyacrylamide gel electrophoresis (Leammli, 1970). The concentration of the purified GSHase was determined spectrophotometrically at 280 nm, using an extinction coefficient of $A^{1\%}_{280nm} = 9.02\ cm^{-1}$ (Kato et al., 1987).

Table 1: Data Collection and Summary of Refinement Results

crystallographic data	
space group	$P6_222$
cell dimensions (Å)	a = 87.25
	b = 87.25
	c = 169.58
unique reflections [$I \geq 2\sigma(I)$]	23410
highest resolution (Å)	1.8
R_{merge}[a] (%)	5.8
completeness (%) (∞−2.0 Å)	79
completeness (%) (2.2−2.0 Å)	51
refinement statistics	
starting model	loopless mutant[b]
initial R-factor[c,d] (%)	32.1
final R-factor[d] (%)	18.8
resolution range (Å)	8.0−2.0
water molecules	136
RMS of bond lengths (Å)	0.012
RMS of bond angle (deg)	2.79

[a] $R_{merge} = 100[\Sigma\Sigma|I(H)_i - \bar{I}(h)|/\Sigma\bar{I}(h)]$. [b] Coordinates of the loopless mutant used for the starting model were obtained from the Brookhaven Protein Data Bank. The entry code is 1GLV. [c] Resolution range is 8.0−2.5 Å. [d] The R-factor is defined by $R = 100[\sum||F_o| - |F_c||/\sum|F_o||]$ calculated with X-PLOR.

Crystals of the unliganded GSHase were obtained in 50 mM Tris-HCl buffer (pH 7.5) containing 25% saturated ammonium sulfate, 5 mM $MgCl_2$, 10 mM 2-mercaptoethanol, and 0.02% NaN_3 by a microdialysis method described previously (Kato et al., 1989). Hexagonal crystals of the unliganded enzyme appeared within 1 week at 25 °C. Complex crystals were produced by soaking unliganded crystals in 50 mM Tris-HCl buffer (pH 7.5), containing 30% saturated ammonium sulfate, 5 mM $MgCl_2$, 5 mM ADP, and 2 mM GSH at 25 °C for 3 days. These crystals have a space group of $P6_222$ and unit cell dimensions of a = 87.25 Å, b = 87.25 Å, and c = 169.58 Å (Table 1).

Data Collection and Reduction. X-ray diffraction data of the complex crystals were collected using the screenless Weissenberg camera for macromolecular crystallography (Sakabe, 1983, 1991), at the beam line $6A_2$ of the Photon Factory, National Laboratory for High Energy Physics (Tsukuba, Japan). The camera radius was 429.7 mm, and the wavelength was fixed at 1.04 Å. All data collections were carried out at 10 °C. One crystal was used for data collection along the a*-axis and another one for the c*-axis. Diffraction patterns were recorded on Fuji BASIII imaging plates (Fuji Film Co. Ltd., Tokyo, Japan) and were digitized using a BA100 scanner (Fuji Film Co. Ltd., Tokyo, Japan). Data were indexed and processed with the WEIS program (Higashi, 1989). Data for each axial setting were merged and scaled individually, followed by merging two data sets into a unique reflection set. In total, 196 511 reflections were observed. Data with $I \geq 2\sigma(I)$ were merged to give a unique data set of 23 410 reflections. The R_{merge} based on intensity was 5.8%, and the completeness was 79% to 2.0 Å resolution. Statistics of the data are shown in Table 1.

Crystallographic Refinement. The crystal of the complex is isomorphous with the loopless mutant. The model of the mutant has an R-factor of 20.7% at 2.7 Å resolution and reasonably good geometry (Kato et al., 1994). This model was used as the starting model for the refinement of the complex, using X-PLOR (Brünger, 1992). In the first step, a rigid body refinement was performed with data between

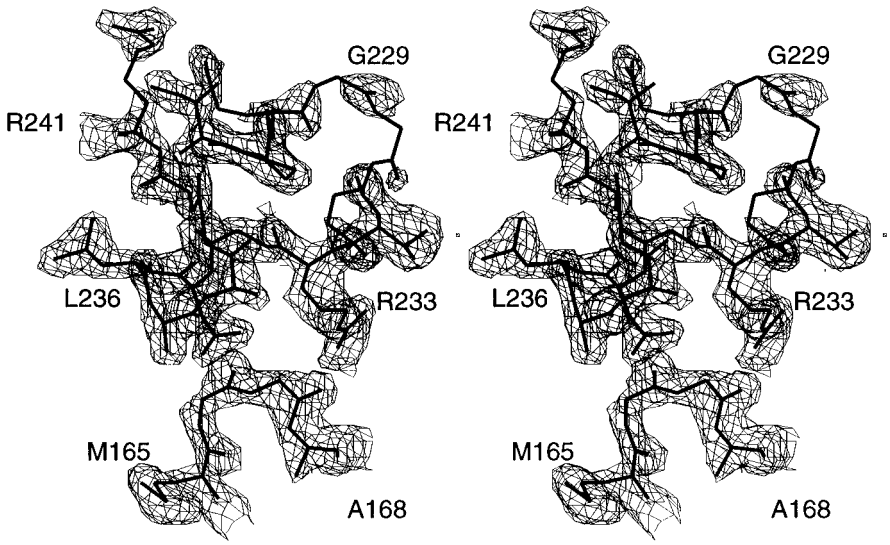

FIGURE 1: Stereoview of the final $2F_o - F_c$ map for the two loop regions covering the active site. These loops (Gly164−Gly167 and Ile266−Arg241) are disordered in the unliganded enzyme. The map is contoured at the 1.0 σ level.

8.0 and 2.5 Å resolution, lowering the starting *R*-factor from 32.1% to 29.6%. Further refinement was carried out using simulated annealing (SA) and conjugate gradient positional refinement. Annealing from 3000 to 300 K lowered the *R*-factor to 22.1%. At this stage, $2F_o - F_c$ and $F_o - F_c$ difference Fourier maps were calculated and examined with FRODO (Jones, 1978). From these two maps, it was possible to build two of the ligands, ADP and GSH, into the model. In addition, two extended stretches of density were evident in the difference Fourier maps, which could be modeled for loops Gly164−Gly167 and Ile226−Gly241. These were missing in the starting model as well as in the crystal structure of the unliganded GSHase (Yamaguchi et al., 1993). Further SA refinement followed by the positional refinement lowered the *R*-factor to 20.3%. A new map calculated at this stage allowed the identification of one of the magnesium ions, which was added to the model. At the next stage, resolution was extended to 2.0 Å, and SA refinement, positional refinement, and *B*-factor refinement were carried out followed by map inspection. At this stage, the geometry of the peptide bond between Val113 and Asn114 was rebuilt to be of *cis* configuration. The density for the last two residues in the sequence, Gln315 and Gln316, was very weak, and these residues were deleted from the model. Several peaks were evident in the difference Fourier maps and assigned as an additional magnesium ion, a sulfate ion, and water molecules. Criteria for the assignment of water molecules were to have at least two possible hydrogen bonds and a distance to hydrogen donor/acceptor from 2.8 to 3.4 Å. Correctness of the assigned water molecules was checked after individual atomic *B*-factor refinement, and those which have *B*-factors greater than 50 Å^2 were excluded from the model. Accuracy of the model of ADP, GSH, two magnesium, and the sulfate was confirmed by an omit map.

RESULTS

Quality of the Structure. The final model containing ADP, GSH, two magnesium ions, and a sulfate ion at the active site was refined to an *R*-factor of 18.8% for all observed reflections between 8.0 and 2.0 Å resolution. The maximum coordinate error of the refined structure of the complex was 0.22 Å as estimated from a Luzzati plot (Luzzati, 1952).

The final model of all the main-chain atoms except for two C-terminal residues, Gln315 and Gln316, is well defined in the $2F_o - F_c$ electron density map at the 1σ level. Two loops (the small loop, Gly164−Gly167, and the large loop, Ile266−Arg241), which are not modeled in the unliganded GSHase structure, were visible in the electron density map and were built in the model of the complex successfully (Figure 1). ADP, GSH, sulfate, and Mg^{2+} ions were well defined in the omit map calculated with the final model excluding those ligands (Figure 2).

The final model has good stereochemistry as judged by geometrical analysis using PROCHECK (Laskowski et al., 1993). The RMS deviations from target values are 0.012 Å for bond lengths and 2.79° for bond angles (Table 1). The main-chain torsion angles, ϕ and ψ, were analyzed by Ramachandran plot; 91.5% out of 247 non-glycine residues are in the theoretically favorable regions of the diagram. Two unusual main-chain structures were observed in the refined structure. Ser155 is outside the permitted region of the Ramachandran plot, and its (ϕ, ψ) angles are (69.8°, −43.0°). This main-chain structure was also observed in the unliganded GSHase structure (Yamaguchi et al., 1993). The Val113−Asn114 peptide bond was identified to be *cis* by inspection of the electron density maps, and this *cis* configuration was retained until the whole refinement procedure was completed. The final model of the complex shows continuous electron density around the *cis* peptide bond. The tetrapeptide segment, Ile112−Lys115, including the *cis* amide bond is in an extensively curved conformation with no intrasegment hydrogen bonds but with seven direct hydrogen bonds with surrounding peptide chains and three water-mediated hydrogen bonds for the stabilization of this unusual structure.

Flexible Loops. The large and small loops make a closed conformation, covering the ADP- and GSH-binding sites completely. The last two residues of the small loop, Gly166 and Gly167, are part of a type I β-turn (Gly166−Ser169). Four residues of the large loop, Leu236−Gly239, form a single turn in a 3_{10}-helix (Figures 1 and 3). Average *B*-factors for main-chain atoms of the small and large loops are 31.5 and 35.9 Å^2, respectively, whereas the average *B*-factor for other main-chain atoms is 19.6 Å^2. End regions

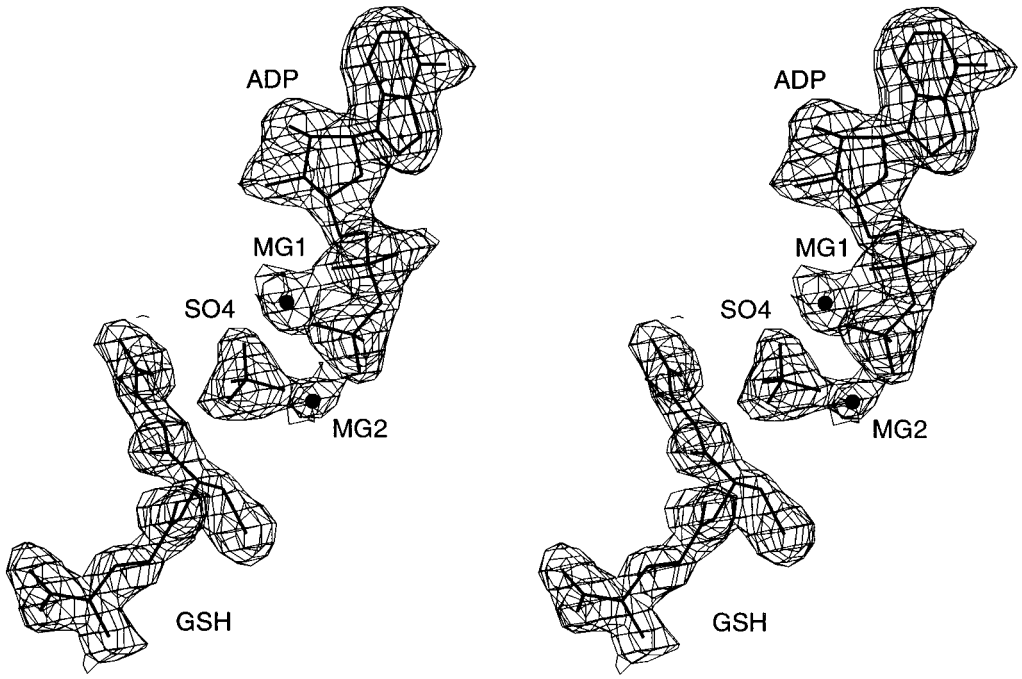

FIGURE 2: Stereoview of the electron density for the ligands, including ADP, GSH, two Mg^{2+} ions, and a sulfate ion at the active site. The $F_o - F_c$ omit map, contoured at the 2.8 σ level, was calculated with the final model excluding the ligands.

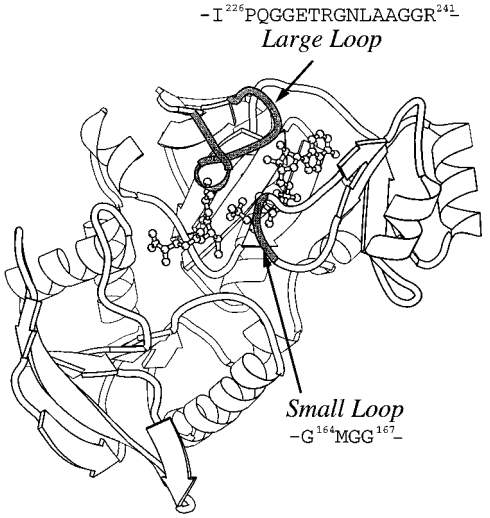

FIGURE 3: Ribbon drawing of a monomeric structure of the quaternary complex. Bound ADP, GSH, two Mg^{2+} ions, and a sulfate ion are illustrated in ball-and-stick models. The two flexible loops, the large loop, and the small loop are shown in gray, and the primary structures of the loops are also indicated in the illustration. The ribbon diagram was generated by MOLSCRIPT (Kraulis, 1991).

of the large loop (Pro227−Glu231 and Ala238−Arg241) have higher *B*-factors than its middle region (Thr232−Ala237). The high *B*-factors, more than 45.0 Å^2, are responsible for the absence of electron density in portions of the region (Gly229−Glu231) in Figure 1.

In the closed conformation, the two loops make numerous polar interactions. These fall into four categories: interactions (i) within the loops (intraloop), (ii) between the large and the small loops (interloop), (iii) between other parts of the protein, and (iv) between the loops and the bound ligands, including solvent waters (Table 2). These polar interactions seem to contribute to the closed conformation of the two flexible loops. Of these interactions, hydrogen bonds observed in the tripeptide segment Glu231−Arg233 are of particular note, since this segment shows the smaller *B*-factor values in the middle of the large loop than the two terminal regions of the loop. The tripeptide segment forms a complicated hydrogen-bonding network mainly with the protein as listed in Table 2.

Table 2: Possible Polar Interactions of Two Flexible Loops[a]

	residue	atom	atom	residue[b]	distance (Å)
interloop	Gly167	O	N_ϵ	Arg233	3.0
	Gly167	O	$N_{\eta 2}$	Arg233	3.1
intraloop	Met165	O	N	Gly167	3.3
	Ile226	N	O	Arg241	2.9
	Glu231	$O_{\epsilon 1}$	N	Thr232	3.0
	Glu231	$O_{\epsilon 2}$	$N_{\eta 1}$	Arg233	2.9
	Asn235	O	N	Ala238	2.9
		O	N	Gly240	2.8
	Leu236	O	N	Gly239	2.9
loop−ligand	Gly166	N	$O_{1\beta}$	ADP	3.3
		N	O_2	sulfate	3.2
		N	O_3	sulfate	3.1
	Gly167	N	$O_{1\beta}$	ADP	2.8
	Gly234	N	$O_{2'}$	ADP	2.8
	Asn235	$N_{\delta 2}$	$O_{3\beta}$	ADP	2.8
		$N_{\delta 2}$	O_3	sulfate	2.9
	Leu236	N	O_{32}	GSH	3.1
	Ala237	N	O_{31}	GSH	3.4
loop−others	Gly164	N	N_ζ	Lys125	2.9
		N	O_w	Wat493	3.0
		O	O_w	Wat440	3.2
		O	O_w	Wat493	3.0
	Gln228	N	O_w	Wat428	2.9
	Thr232	$O_{\gamma 1}$	O	Pro178*	2.6
		$O_{\gamma 1}$	O_w	Wat498	3.1
	Arg233	$N_{\eta 1}$	$O_{\epsilon 2}$	Glu185*	2.8
		$N_{\eta 2}$	O_w	Wat496*	3.0
	Asn235	$N_{\delta 2}$	O_w	Wat458	2.9
	Gly240	N	O_w	Wat486	3.3
	Arg241	$N_{\eta 2}$	$O_{\epsilon 2}$	Glu243	3.2

[a] Polar bonds in the two flexible loops shorter than 3.4 Å in the quaternary complex are reported. [b] The residues marked by asterisks belong to the other contacting subunit.

Binding of ADP. ADP binds on the face of the β-sheet in the central domain and stretches along two β-strands con-

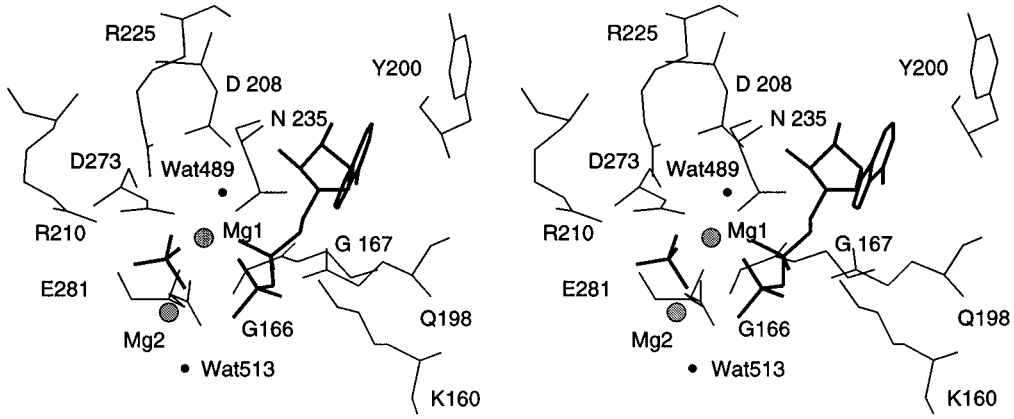

FIGURE 4: Stereoview of the ADP-binding site. ADP is illustrated in thick lines. Solvent molecules are indicated as dots. The gray balls are the two Mg^{2+} ions.

Table 3: Possible Polar Interactions of ADP[a]

	atom	atom	residue	distance (Å)
base	N_6	$O_{\epsilon 1}$	Gln198	3.0
	N_6	O	Asn199	3.1
		$O_{\epsilon 1}$	Gln198	3.2
sugar	$O_{2'}$	O	Thr232	2.9
		N	Gly234	2.8
	$O_{3'}$	$O_{\delta 2}$	Asp208	2.6
		N	Gly234	3.4
α-phosphate	$O_{1\alpha}$	Mg	Mg1	2.0
		O_w	Wat445	2.6
		O_w	Wat458	2.9
	$O_{2\alpha}$	N_ζ	Lys160	2.7
		O_w	Wat445	3.2
β-phosphate	$O_{1\beta}$	N	Gly166	3.3
		N	Gly167	2.8
		O_w	Wat489	2.9
	$O_{2\beta}$	N_ζ	Lys125	3.1
		Mg	Mg2	2.8
		O_w	Wat513	3.0
	$O_{3\beta}$	$N_{\delta 2}$	Asn235	2.8
		Mg	Mg1	2.2
		O_w	Wat458	3.0

[a] Polar bonds between the bound ADP and the protein shorter than 3.4 Å in the quaternary complex are reported.

nected by the small loop (Figure 3). The geometry of the bound ADP is major $C_{3'}$-*end*−minor $C_{2'}$-*exo* for the ribose ring pucker and *anti* conformation for the glycosidic bond (Figures 2 and 4). As listed in Table 3, the bound ADP forms many polar interactions with the protein. The adenine ring is buried in a hydrophobic pocket of the cleft and makes three polar contacts with the protein: N_6 with $O_{\epsilon 1}$ of Glu198 and with O of Asn199 and N_7 with O_{e1} of Gln198. Ile158, Ile170, Tyr200, Ile204, and Ile245 provide a hydrophobic environment around the adenine ring in the binding pocket. Although Tyr200 is about 3.6 Å apart from the adenine ring, no interplane stacking is observed between the adenine ring and the phenyl ring of Tyr200 (Figure 4). The hydroxyl group in the 2′ position of the sugar forms a hydrogen bond with the main-chain amide of Gly234 on the large loop. A polar interaction between the 3′-OH group and $O_{\delta 2}$ of Asp208 is also observed. The α-phosphate oxygens make hydrogen bonds with the N_ϵ atom of Lys160 as well as with waters Wat445 and Wat458 which interact with $O_{\gamma 1}$ of Thr280 and with $N_{\delta 2}$ of Asn235, respectively. The β-phosphate makes hydrogen bonds with main-chain N atoms of Gly166 and Gly167 on the small loop and with the N_ϵ atom of Lys125. Wat489 and Wat513 interact with the β-phosphate oxygens forming hydrogen bonds (Figure 4).

Bound Ions. The electron density shows very clearly the two Mg^{2+} ions which are located close to the phosphate moiety of ADP (Figure 2). Mg1 has an octahedral coordination geometry with six ligands: α- and β-phosphate oxygens ($O_{1\alpha}$ and $O_{2\beta}$), $O_{\delta 2}$ of Asp273, $O_{\epsilon 2}$ of Glu281, one oxygen of the sulfate ion, and a solvent oxygen from Wat458 with distances between 1.9 to 2.2 Å (Figure 5). In contrast, Mg2 has a distorted octahedral geometry with unusual coordination by six oxygen atoms: $O_{\epsilon 1}$ and $O_{\epsilon 2}$ of Glu281, $O_{\delta 1}$ of Asn283, $O_{2\beta}$ of β-phosphate, the other oxygen of the sulfate ion, and a solvent oxygen of Wat513. The distances of the six oxygen ligands from Mg2 are between 1.9 and 2.7 Å (Figure 5).

The sulfate ion was built into well-defined tetrahedral electron density in the active site. The bound sulfate is likely to come from the precipitant (ammonium sulfate) used for crystallization. The sulfate in the quaternary complex is located between the β-phosphate of ADP and the amide carbon of the cysteinyl−glycyl peptide moiety of GSH (Figure 2). Arg210 and Arg225 make electrostatic interactions with the sulfate. The sulfate makes hydrogen bonds with the main-chain amide of Gly166 and with $N_{\delta 2}$ of Asn235. Two of the oxygens of the sulfate are ligands to the two Mg^{2+} ions (Figure 5). The sulfate ion seems to be trapped in a desolvated form in the active site. There are no water molecules which make contact with it.

Glutathione-Binding Site. The GSH molecule is bound at the active site of GSHase in an extended conformation across a loop of Asn283−Cys289. The main chain of the loop seems to sink at Pro287 and interlock with the GSH molecule. There are 17 hydrogen bonds and electrostatic interactions between the GSH molecule and the active site of the enzyme (Figure 6).

The interactions between the γ-glutamyl moiety of GSH and the enzyme are of special interest. Two oxygens of the α-carboxylate of the γ-glutamyl moiety interact with $N_{\eta 2}$ of Arg86 and with $O_{\gamma 1}$ of Thr288. The interaction between $N_{\eta 2}$ of Arg86 and the α-carboxylate of the γ-glutamyl moiety seems to be weak, since only one hydrogen bond is formed between the guanidino group of Arg86 and the substrate. The bound α-carboxyl group is located near the N-terminal end of helix Ser20−Arg31, forming hydrogen bonds with backbone amides of Ser20 and Ser21 in the first turn of the helix (Figure 3). Binding of the α-carboxylate seems to be thus assisted by these hydrogen bonds. The α-amino group

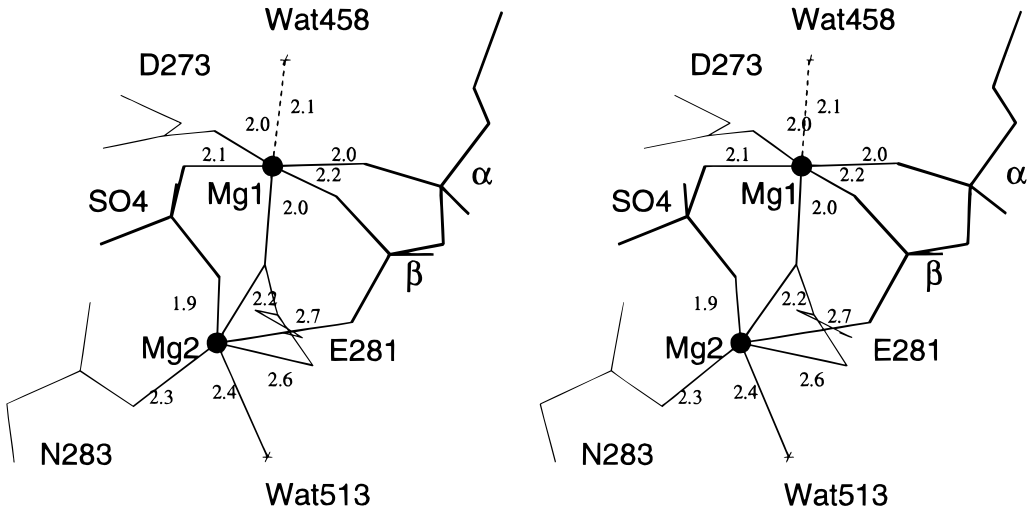

FIGURE 5: Stereoview of the Mg^{2+} ion-binding site. Mg^{2+} ions are represented by gray balls. Solvent molecules are illustrated as crosses. The coordination geometry of each Mg^{2+} ion is illustrated in dashed lines with the distances marked in angstroms.

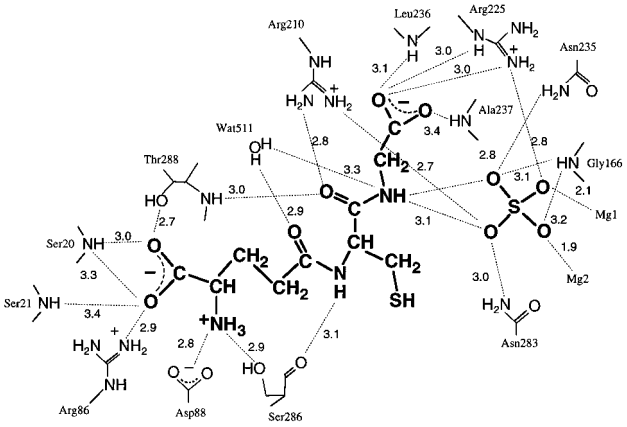

FIGURE 6: Schematic diagram for the interactions between the enzyme and GSH, the bound sulfate ion, and the ordered water molecules at the active site. The interactions are illustrated in dashed lines with distances (≤3.4 Å).

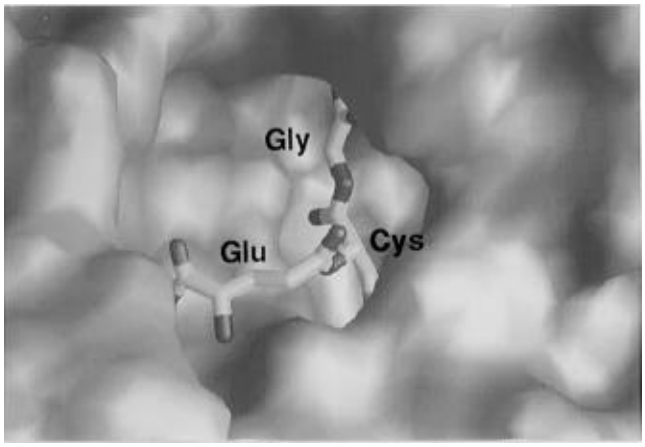

FIGURE 7: Surface representation of the GSH-binding site. The diagram was generated using the program GRASP (Nicholls et al., 1991). The surface of the large loop region is colored in emerald green. GSH is shown as a stick model. The view is the same as in Figure 3.

of the γ-glutamyl moiety forms polar interactions with $O_{\delta1}$ of Asp88 and with O_γ of Ser286.

The oxygen and nitrogen atoms of the amide bond between the γ-glutamyl and cysteinyl groups make contact with the carbonyl oxygen of Ser286 and with Wat511, respectively (Figure 6). There are no significant polar interactions between the sulfhydryl group of GSH and the enzyme. The sulfhydryl group is surrounded by Pro89 and Met165, forming van der Waals contacts.

There are several interactions with the amide moiety of the Cys−Gly part of GSH. As shown in Figure 6, the carbonyl oxygen is hydrogen bonded with $N_{\eta2}$ of Arg210 and with N of Thr288. The nitrogen atom of the Cys−Gly amide bond makes polar interactions with one of the sulfate oxygens.

The glycyl moiety is located in the N-terminal part of the 3_{10}-helix of the large loop (Asn235−Ala237) and the side chains of Arg210 and Arg225. The binding site of the glycyl moiety forms a rather narrow pocket (Figure 7). There seems to be no room for bulky groups substituted at the C_α position of the glycyl moiety to enter the pocket. The terminal carboxylate of the glycyl moiety forms hydrogen bonds with the main-chain amides of Ala236 and Leu237 on the large loop and the side-chain amide of Arg225 (Figure 6). It is likely that the binding pocket for the glycyl moiety is responsible for strict substrate specificity in GSHase with respect to glycine (Moore & Meister, 1987; Kato et al., 1994).

Comparison of the Active Site Structure between the Quaternary Complex and the Unliganded Enzyme. The structure of the quaternary complex is almost identical to the structure of the unliganded GSH. Superposition of C_α positions gives an RMS difference of 0.44 Å. When the side-chain structures of the two GSHase forms are compared, significant spatial rearrangements can be observed, especially at the active site. Most of these rearrangements are due to interactions with ADP, GSH, the two Mg^{2+} ions, and the bound sulfate. Arg210, Arg225, and Asn283 move drastically, showing maximum displacement distances of 4.4, 7.2, and 5.7 Å, respectively (Figure 8). Asn283 rotates around the β-position to contact Mg1 (Figure 8). Besides, Glu124, Lys125, and Glu281 move to form direct- and water-mediated hydrogen bonds with the ligands.

DISCUSSION

The Pseudo Enzyme−Substrate Complex in the Reverse Reaction. The crystal structure of the quaternary complex including GSHase, ADP, GSH, and sulfate simulates the

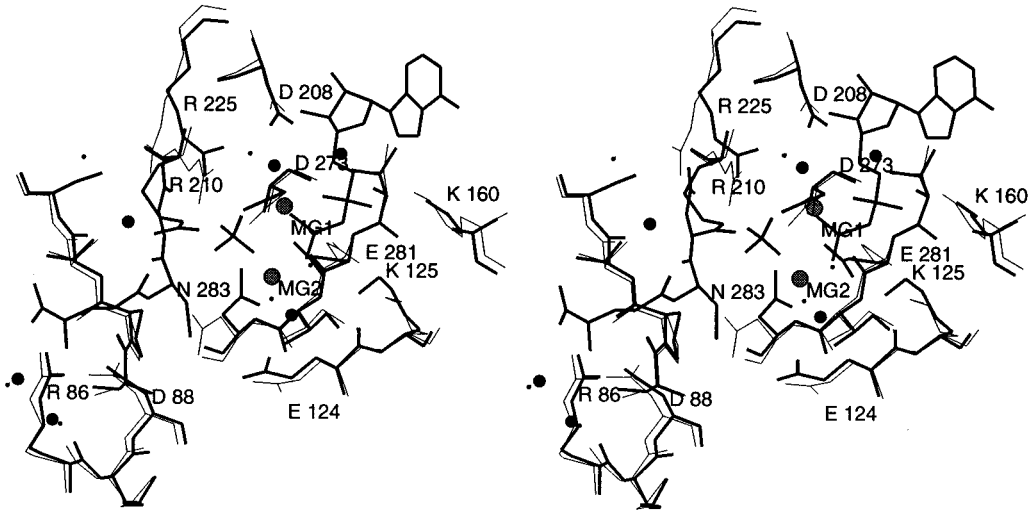

FIGURE 8: Stereoview of the active site structure of the quaternary complex (thick lines, this work) superposed on the structure of the unliganded GSHase (thin lines; Yamaguchi et al., 1993). The large dots are water molecules in the quaternary complex structure, and the small dots are water molecules from the unliganded GSHase. The bound Mg^{2+} ions are illustrated in gray balls.

structure of the enzyme−product complex comprising GSHase, ADP, GSH, and phosphate. This quaternary complex can be considered as a pseudo enzyme−substrate complex (E−S complex) in the reverse reaction of GSHase. It is likely that the sulfate in the complex occupies the phosphate-binding site in the enzyme. Enzymatic activity is inhibited by sulfate in solution, and in the presence of 1.5 M ammonium sulfate, the relative activity of GSHase is only 14.5% of the activity without sulfate (unpublished results). The bound sulfate in the crystal structure of the quaternary complex is located between the β-phosphate of ADP and the carbon atom in the Cys−Gly amide of GSH (Figure 2). The β-phosphate of ADP, the sulfate, and the carbon are almost in line. This arrangement should be needed for the phosphoryl transfer of γ-phosphate from ATP to the C-terminal carboxylate of γ-Glu-Cys via a pentacoordinated transition state. Copley and Barton (1994) indicated that the chemical properties of phosphate and sulfate are sufficiently similar to allow the two groups to bind in locations with similar properties. Accordingly, all locations found to bind sulfate ions must also be viewed as potential phosphate binding sites (Copley & Barton, 1994). On the basis of chemical and crystallographic evidence, it is very likely that the position of the bound sulfate in the present quaternary complex mimics the position of the phosphate generated from the γ-phosphate of ATP in the forward reaction. There are two Mg^{2+} ions lying at the active site in the quaternary complex. Mg1 interacts with α- and β-phosphate of ADP and the sulfate ion whereas Mg2 is interacted with β-phosphate of ADP and the sulfate ion. It is thus likely that both magnesium ions interact with the γ-phosphate of ATP in the real E−S complex of GSHase.

Previous crystallographic studies on the binary and ternary E−S complexes of *E. coli* GSHase (Yamaguchi et al., 1993) show disordered active site structures. The present quaternary pseudo E−S complex is stable enough to allow a detailed crystallographic analysis of the active site and the bound ligands. The results indicate that a central quaternary E−S complex is likely to exist in the enzymatic reaction with a stable conformation to accelerate the reaction. How much of the structure is ordered may depend on the position along the reaction coordinate. Flexibility in the E−S complex might be much reduced at any of the transition states. Recent studies by Hiratake et al. (1994) suggest that GSHase shows more reduced conformational flexibility near the transition state than in the E−S complex (personal communication). In the reversible enzymatic reaction, the E−S complex could release either the substrate or the product in the next reaction step, or it could go along the catalytic pathway through a transition state. The E−S complex structure should be flexible enough in order to permit substrate/product binding and release, while remaining stable enough to approach the transition state.

Active Site Architecture of GSHase. The negatively charged ligands at the active site of the *E. coli* GSHase are stabilized by interactions with main-chain NH groups and positively charged arginine and lysine side chains. Interactions of the substrate with the main-chain NH groups include (i) the first turn of the α-helix, the NH groups of Ser20 and Ser21 interact with the α-carboxylate of the glutamyl moiety of GSH, (ii) Leu236 and Ala237 of the 3_{10}-helix of the large loop interact with the carboxylate of the glycine moiety, and (iii) two glycine residues, Gly166 and Gly167, in the small loop interact with the β-phosphate of ADP and with the bound sulfate ion (Figures 3 and 6). The advantage of using the NH groups at the helix terminal is precision in positioning ligands because of the structural rigidity of the helices (Quiocho et al., 1987; Knowles, 1991). It is also considerable that the helix dipole would contribute to the interaction with the charged ligands. Both helices that interact with the bound ligands function to fix the positions of the substrates and products. The two NH groups in the small loop serve as an anchor to hold the phosphate groups of the nucleotide: Gly166 mainly for γ-phosphate and Gly167 for the β-phosphate. To ensure the progress of the reaction, the use of the flexible loops and the main chain NH groups seems to be more advantageous than using flexible side chains to control the orientation of the ligands. The enzyme must grip the phosphate moieties during the reaction even after the cleavage of the $\beta-\gamma$ pyrophosphate bond. Thus, the active site in GSHase needs to be a functional unit which possesses a mobility to adopt the transient structures of the phosphate moieties and a rigidity to regulate their right positions.

GSHase uses two arginines (Arg225, Arg210) and one lysine (Lys160) to stabilize the negatively charged transition states. Arg225 is a candidate to stabilize the pentacoordinated phosphoryl group during phosphoryl transfer, and Arg210 is ideally placed to provide a guanidino group to stabilize the tetrahedral adduct when the substrate glycine attacks the acylphosphate intermediate. Arg210 also would act as an anchor for the C-terminal carboxylate of γ-Glu-Cys in the substrate binding event. Lys160 is bound to the α-phosphate of the nucleotide and directs the β- and γ-phosphate groups during catalysis. Compared to main-chain NH groups, arginine and lysine residues suffer from entropic disadvantages in stabilizing ligands because of their extreme flexibility. The flexible side chains of these positively charged residues are fixed by a complicated network of many polar interactions in the active site of GSHase. Lys160 is in a network including the side chain of Gln198 and the N_6 atom of adenine ring, while Arg225 and Arg210 are held by interactions with Asp208 and Asp273, respectively (Figure 7). These aspartate residues are involved in the nucleotide binding via the direct interaction or the indirect interaction with the magnesium ion, Mg1.

The structure of the quaternary complex of the enzyme in the pseudo-Michaelis complex reveals, for the first time, the active site architecture of this enzyme and the structure of the bound products. The active site architecture is illustrative for its employment of the peptide units as helices and loops in the catalytic events.

ACKNOWLEDGMENT

We thank Drs. N. Sakabe, A. Nakagawa, and N. Watanabe for their advice and help in data collection at the Photon Factory, National Laboratory for High Energy Physics, Tsukuba, Japan. We also thank Drs. T. Nishioka and A. Kimura, Kyoto University, and H. Yamaguchi, Osaka University, for their assistance with various aspects of this work and J. Hiratake for many helpful discussions. The computing support by the Super Computer Laboratory, Institute for Chemical Research, Kyoto University, is gratefully acknowledged.

SUPPORTING INFORMATION AVAILABLE

Illustration of stereoviews of the electron density map around the *cis* peptide bond (Val113−Thr114) accompanied with the hydrogen bond network (1 page). Ordering information is given on any current masthead page.

REFERENCES

Brünger, T. A. (1992) in *X-PLOR version 3.1: A system for x-ray crystallography and NMR*, Yale University Press, New Haven, CT.

Copley, R. R., & Barton, G. J. (1994) *J. Mol. Biol. 242*, 321−329.

Cusack, S., Colominas, C. B., Härtlein, M., Nassar, N., & Leberman, R. (1990) *Nature 347*, 249−255.

Fan, C., Moews, P. C., Walsh, C. T., & Knox, J. R. (1994) *Science 266*, 439−443.

Gushima, H., Miya, T., Murata, K., & Kimura, A. (1983) *J. Appl. Biochem. 5*, 210−218.

Gushima, H., Yasuda, S., Soeda, E., Yokota, M., Kondo, M., & Kimura, A. (1984) *Nucleic Acids Res. 12*, 9299−9307.

Hara, T., Tanaka, T., Kato, H., Nishioka, T., & Oda, J. (1995) *Protein Eng. 8*, 711−716.

Hibi, T., Kato, H., Nishioka, T., Oda, J., Yamaguchi, H., Katsube, Y., Tanizawa, K., & Fukui, T. (1993) *Biochemistry 32*, 1548−1554.

Higashi, T. (1989) *J. Appl. Crystallogr. 22*, 9−18.

Hiratake, J., Kato, H., & Oda, J. (1994) *J. Am. Chem. Soc. 116*, 12059−12060.

Jones, T. A. (1978) *J. Appl. Crystallogr. 11*, 268−272.

Kato, H., Chihara, M., Nishioka, T., Murata, K., Kimura, A., & Oda, J. (1987) *J. Biochem. (Tokyo) 101*, 207−215.

Kato, H., Tanaka, T., Nishioka, T., Kimura, A., & Oda, J. (1988) *J. Biol. Chem. 263*, 11646−11651.

Kato, H., Yamaguchi, H., Hata, Y., Nishioka, T., Katsube, Y., & Oda, J. (1989) *J. Mol. Biol. 209*, 503−504.

Kato, H., Tanaka, T., Yamaguchi, H., Hara, T., Nishioka, T., Katsube, Y., & Oda, J. (1994) *Biochemistry 33*, 4995−4999.

Knighton, D. R., Zheng, J., Ten Eyck, L. F., Ashford, V. A., Xuong, N.-H., Taylor, S. S., & Sowadski, J. M. (1991a) *Science 253*, 407−414.

Knighton, D. R., Zheng, J., Ten Eyck, L. F., Ashford, V. A., Xuong, N.-H., Taylor, S. S., & Sowadski, J. M. (1991b) *Science 253*, 414−420.

Knowles, J. R. (1991) *Philos. Trans. R. Soc. London, B 332*, 115−121.

Kraulis (1991) *J. Appl. Crystallogr. 24*, 964−950.

Laemmli, U. K. (1970) *Nature 227*, 680−685.

Laskowski, R. A., MacArthur, M. W., Moss, D. S., & Thornton, J. M. (1993) *J. Appl. Crystallogr. 26*, 283−291.

Luzzati, V. (1952) *J. Appl. Crystallogr. 5*, 802−810.

Meek, T. D., & Villafranca, J. J. (1980) *Biochemistry 19*, 5513−5519.

Meister, A. (1988) in *Glutathione: chemical, biochemical, and medical aspects* (Dolphin, D., Paulson, R., & Avramovic, O., Eds.) Part A, pp 387−390, John Wiley & Sons, Inc., New York, NY.

Moore, W. R., & Meister, A. (1987) *Anal. Biochem. 161*, 487−493.

Mullins, L. S., Zawadzke, L. E., Walsh, C. T., & Raushel, F. M. (1990) *J. Biol. Chem. 265*, 8993−8998.

Nicholls, A., Sharp, K., & Honig, B. (1991) *Proteins: Struct., Funct., Genet. 11*, 281−296.

Quiocho, F. A., Sack, J. S., & Vyas, N. K. (1987) *Nature 329*, 561−564.

Ruff, M., Krishnaswamy, S., Boeglin, M., Poterszman, A., Mitschler, A., Podjarny, A., Rees, B., Thierry, J. C., & Moras, D. (1991) *Science 252*, 1682−1689.

Sakabe, N. (1983) *J. Appl. Crystallogr. 16*, 542−547.

Sakabe, N. (1991) *Nucl. Instrum. Methods A303*.

Tanaka, T., Kato, H., Nishioka, T., & Oda, J. (1992) *Biochemistry 31*, 2259−2265.

Tanaka, T., Yamaguchi, H., Kato, H., Nishioka, T., Katsube, Y., & Oda, J. (1993) *Biochemistry 32*, 12398−12404.

Yamaguchi, H., Kato, H., Hata, Y., Nishioka, T., Kimura, A., Oda, J., & Katsube, Y. (1993) *J. Mol. Biol. 229*, 1083−1100.

BI9605245